



LUND UNIVERSITY

Temporally and spectrally resolved images of single burning pulverized wheat straw particles

Weng, Wubin; Costa, Mário; Li, Zhongshan; Aldén, Marcus

Published in:
Fuel

DOI:
[10.1016/j.fuel.2018.03.101](https://doi.org/10.1016/j.fuel.2018.03.101)

2018

Document Version:
Publisher's PDF, also known as Version of record

[Link to publication](#)

Citation for published version (APA):
Weng, W., Costa, M., Li, Z., & Aldén, M. (2018). Temporally and spectrally resolved images of single burning pulverized wheat straw particles. *Fuel*, 224, 434-441. <https://doi.org/10.1016/j.fuel.2018.03.101>

Total number of authors:
4

Creative Commons License:
CC BY-NC-ND

General rights

Unless other specific re-use rights are stated the following general rights apply:
Copyright and moral rights for the publications made accessible in the public portal are retained by the authors and/or other copyright owners and it is a condition of accessing publications that users recognise and abide by the legal requirements associated with these rights.

- Users may download and print one copy of any publication from the public portal for the purpose of private study or research.
- You may not further distribute the material or use it for any profit-making activity or commercial gain
- You may freely distribute the URL identifying the publication in the public portal

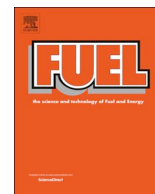
Read more about Creative commons licenses: <https://creativecommons.org/licenses/>

Take down policy

If you believe that this document breaches copyright please contact us providing details, and we will remove access to the work immediately and investigate your claim.

LUND UNIVERSITY

PO Box 117
221 00 Lund
+46 46-222 00 00



Full Length Article

Temporally and spectrally resolved images of single burning pulverized wheat straw particles

Wubin Weng^a, Mário Costa^{b,*}, Zhongshan Li^a, Marcus Aldén^a

^a Division of Combustion Physics, Lund University, P. O. Box 118, S 221 00 Lund, Sweden

^b IDMEC, Mechanical Engineering Department, Instituto Superior Técnico, Universidade de Lisboa, Lisboa, Portugal



ARTICLE INFO

Keywords:

Biomass
Wheat straw
Single particle combustion
Temporally and resolved images
Chemiluminescence

ABSTRACT

This work focuses into the combustion behaviour of single wheat straw particles with the aim of providing a quantitative description of the particle burning process from ignition to the early stages of the char oxidation. The single particles, in the size range 224–250 μm , were injected upward into a confined region with hot combustion products, produced by a flat flame McKenna burner, with a mean temperature of 1550 K and a mean dry O_2 concentration of 6.5 vol%. Spectral emission data and temporally resolved images of the single burning particles were obtained with a spectrometer and an ICCD camera, respectively. To obtain spectrally resolved images the camera was equipped with different band-pass filters. Overall, the results demonstrate the ability of the present experimental setup and associated optical diagnostics to gather quantitative information of the combustion process of single pulverized solid fuel particles. The emission spectra from the burning wheat straw particles showed that the emission was mainly originated from CH^* , C_2^* , Na^* and K^* chemiluminescence, and thermal radiation from soot and char burning particles. The ICCD images show that the emission from excited CH , C_2 , Na and K is initially detected almost at the same time, the burning of the soot particles initiates soon after the ignition, and the char particles experience ignition after the extinction of the homogeneous combustion. During the volatiles combustion stage, the temporal evolution of the normalized emission intensity of the excited CH , C_2 , atomic sodium and atomic potassium is quite similar; during the char oxidation stage, however, the decrease of the emission intensity of the excited atomic sodium and potassium is delayed in relation to the decrease in the emission intensity of CH and C_2 because of the continuous release of atomic sodium and potassium from the burning char particles.

1. Introduction

Despite the great attention that the use of pulverized biomass in combustion processes has attracted in recent years, notably in co-firing with coal, this interest has not promoted a significant increase in the number of fundamental studies on biomass combustion. One reason for this is presumably the conviction that fossil fuels, particularly coal, will remain the main source of power generation in the next decades. Nonetheless, the reduction of the greenhouse gas emissions demands an increasing use of biomass so that it is essential to rapidly reduce the gap between the current superior knowledge on pulverized coal combustion and that on pulverized biomass combustion, recognizing the similarities between the two cases, but identifying and deepening the differences. The perception of these differences is fundamental for the design of new burners for both pure biomass firing and co-firing biomass with coal and thereby to increase the use of biomass in combustion processes.

The study of basic reaction processes such as particle heating, pre-ignition and ignition behavior, devolatilization, combustion of the volatiles and char oxidation is commonly performed in single particle experiments under laminar flow conditions or low levels of turbulence. These experiments allow the use of optical diagnostics to measure particle size and temperature, flame luminosity and chemiluminescent emission from various radicals. On the pulverized coal side, Shaddix and Molina [1] used an intensified charge-coupled device (ICCD) camera to investigate the ignition and devolatilization of single coal particles during oxy-fuel combustion, Levendis and co-workers [2–6] employed three-color pyrometry and high-speed high-resolution cinematography to study the ignition and combustion of single coal particles in O_2/N_2 and O_2/CO_2 atmospheres, Köser et al. [7] used planar high-speed laser-induced fluorescence of OH to examine the ignition and volatile combustion of single coal particles in oxygen-enriched environments, and Bai et al. [8] employed a high-speed video camera

* Corresponding author.

E-mail address: mcosta@ist.utl.pt (M. Costa).

<https://doi.org/10.1016/j.fuel.2018.03.101>

Received 28 August 2017; Received in revised form 13 March 2018; Accepted 14 March 2018

Available online 20 March 2018

0016-2361/ © 2018 The Authors. Published by Elsevier Ltd. This is an open access article under the CC BY-NC-ND license (<http://creativecommons.org/licenses/by-nc-nd/4.0/>).

and image processing techniques to quantify the combustion behavior of single coal particles in terms of size, shape, surface roughness, rotation frequency and luminosity. All these studies provided valuable information on the ignition mechanisms, ignition delay time, volatile matter composition and combustion, soot formation and oxidation and char combustion of single coal particles burning in various atmospheres.

On the pulverized biomass side, Riaza et al. [9] used the techniques employed in Refs. [2–6] to study the combustion behavior of single particles of sugarcane bagasse, pine sawdust, torrefied pine sawdust and olive residue, all in the size range 75–150 μm , in air and O_2/CO_2 atmospheres at a gas temperature of 1400 K; authors concluded that the combustion behavior of the four biomass residues evidenced only small differences based on their origin, type and pre-treatment. Mock et al. [10,11] employed high-speed photography to study the burning behavior of single particles of torrefied wood, coffee waste, sewage sludge and torrefied sewage sludge, in size ranges 150–215 μm , 255–300 μm , 355–425 μm and 425–500 μm , in an atmosphere with O_2 concentrations ranging from 10% to 40% at gas temperatures of 1090 and 1340 K; authors observed different burning characteristics for the various single biomass particles, which they attributed to their different chemical and physical properties. Simões et al. [12] also employed high-speed photography to examine the ignition behavior of single particles of wheat straw, kiwi branches, vine branches, sycamore branches and pine bark, in size ranges 80–90 μm , 212–224 μm and 224–250 μm , in a confined laminar flow of combustion products with O_2 concentrations ranging from 3.5% to 6.5% at gas temperatures ranging from 1500 to 1800 K; authors concluded that ignition of the biomass particles generally occurred in the gas-phase, although surface ignition was also observed.

In contrast with the combustion of single coal particles, the existing information for the combustion of single biomass particles does not include data on the temporal evolution of excited species in the flame. Therefore, this work focuses into the combustion behavior of single biomass particles with the aim of providing a quantitative description of the particle burning process from ignition to the early stages of the char oxidation. The single particles were injected upward into a confined region with hot combustion products, produced by a flat flame McKenna burner. Spectral emission data and temporally resolved images of the single burning particles were obtained with a spectrometer and an ICCD camera, respectively. To obtain spectrally resolved images the camera was equipped with different band-pass filters. The manuscript provides new data on particle ignition, volatiles burning, soot formation, alkali species release and early stages of char combustion of single biomass particles.

2. Materials and methods

2.1. Experimental setup and optical diagnostics

Fig. 1a shows a schematic of the experimental setup used. It consists of a biomass feeding unit, a McKenna flat flame burner and an air/methane feeding system. The biomass feeding unit consists of a mass flow controller (to control the transport fluid flow rate), a 10 mL syringe and a vibrating motor. The biomass particles, which are stored in the syringe, are fed (by gravitational force) into a stream of nitrogen (transport fluid) and injected upward through a central hole located in the burner (I.D. 1.55-mm) into the hot combustion products region of the McKenna burner. The vibrating motor avoids the clogging of the biomass particles in the syringe hole and ensures a low feeding rate of particles.

The McKenna flat flame burner consists of a stainless-steel cylinder enveloping a water-cooled bronze porous sintered matrix of 60-mm diameter. Two mass flow controllers allow the control of the methane and primary air flow rates to the burner. In addition, cooling water is fed to the burner through copper tubes. Above the burner, a high-grade fused quartz of I.D. 70-mm, height of 500-mm, and thickness of 2-mm

confines the flow and avoids the entrainment of ambient air, while providing optical access.

Fig. 1b shows a schematic of the optical diagnostics used for the emission spectrum measurements and capture of the images of the single burning particles. The spectral emission data from the single burning particles was obtained with a spectrometer (Andor, SR-750, $f/9.7$) with a 300 lines/mm grating and a 100 μm slit. The temporally resolved images of the single burning particles were obtained with an ICCD camera (Andor, iStar, 1024×1024 pixels) with an exposure time of 500 μs . To obtain spectrally resolved images the camera was equipped with different band-pass filters. Additionally, a stereoscope lens was placed in front of the ICCD camera to allow for the simultaneous capture of images of each particle with two filters. The synchronization between the spectrometer or the ICCD camera and each incoming single particle was achieved with the aid of the signal synchronization system shown in Fig. 1b. This synchronization system also allowed for the calculation of the residence time of each particle in the hot combustion products region produced by the McKenna burner. A 532 nm continuous-wave laser (200 mW) was used to generate a laser beam with a diameter of 1-mm. This laser beam was placed very close to the exit of the central hole located in the McKenna burner through which the particles were injected upward into the hot combustion products region. The scattering signal generated by each single particle crossing the laser beam was collected by a photodiode together with a spherical lens, which triggered the spectrometer or the ICCD camera with a pulse generator (DG535).

2.2. Biomass fuel and test conditions

Table 1 shows the properties of the wheat straw used in this study. The biomass was ground and sieved to a particle size range of 224–250 μm . The McKenna burner was fed with a mixture of CH_4 (1.03 L/min) and air (14.68 L/min). The resulting flat flame, with an equivalence ratio of 0.67, produced a region of hot combustion products, where the particles were injected, with a mean velocity of 0.42 m/s, a mean temperature of 1550 K and a mean dry O_2 concentration of 6.5 vol%. The nitrogen flow rate used to transport the biomass particles was 0.097 L/min.

3. Results and discussion

3.1. Emission spectrum

Fig. 2a shows the emission spectrum of burning pulverized wheat straw particles obtained with the spectrometer, where several emission lines can be recognized. The measured emission lines around 430 nm are identified as the emission from excited CH radicals based on a comparison with the spectral structure of the CH emission from LIF-BASE [13]. In addition, the interference from the broad-band emission is negligible in this short wavelength region. Consequently, the measured signal using the 430 nm band-pass filter (BF430) is mainly attributable to the excited CH radicals of the burning wheat straw particles.

Fig. 2b shows typical images of burning pulverized wheat straw particles obtained with the ICCD camera equipped with different filters for particle residence times in the hot combustion products region of 70 and 120 ms. Note that these two residence times correspond to different moments during the combustion process of the particles; specifically: 70 ms corresponds to an instant when only volatiles combustion takes place and 120 ms to an instant when only char oxidation occurs. In this study, particle ignition started with the ignition of the volatiles released from the particles. The subsequent volatiles oxidation forms a spherical flame front around the particles. Since CH^* (BF430) is a good indicator of the reaction zone, its emission signal represents the flame front, as may be seen in Fig. 2b for a residence time of 70 ms. The flame front has a size of around 2 mm, which is almost 10 times larger than the initial particle diameter. For a residence time of 120 ms, the signal at 430 nm

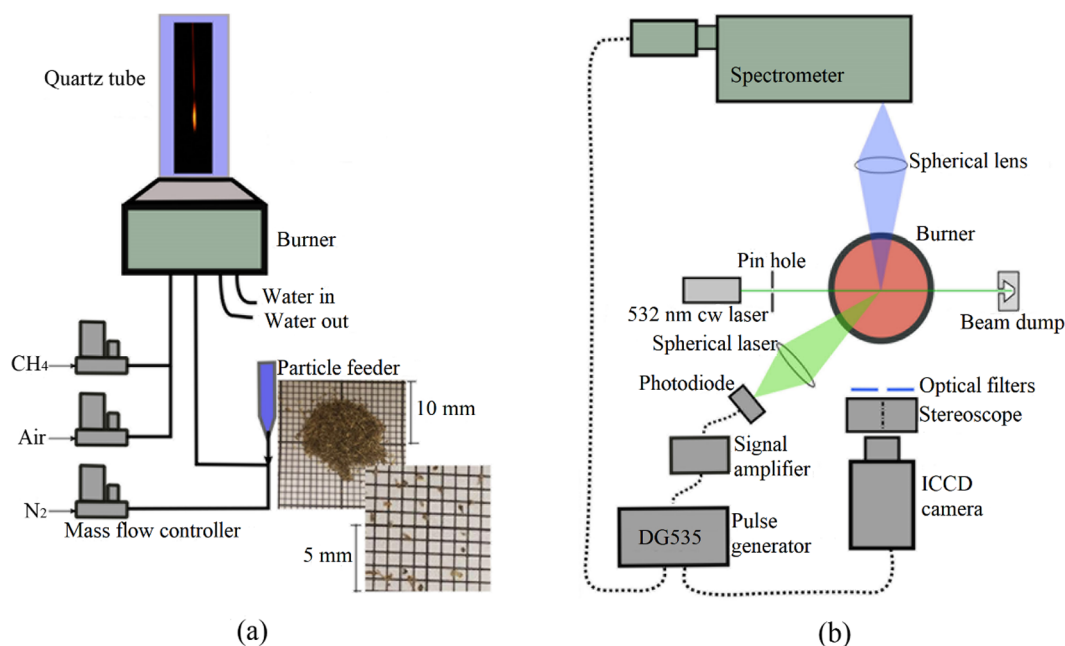


Fig. 1. Schematic views of the (a) experimental setup; and (b) optical diagnostics for the emission spectrum measurements and capture of images of single burning particles.

Table 1
Properties of the wheat straw.

Parameter	Value
<i>Proximate analysis (wt%, as received)</i>	
Volatile matter	64.9
Fixed carbon	12.4
Moisture	8.0
Ash	14.7
<i>Ultimate analysis (wt%, dry ash free)</i>	
Carbon	41.1
Hydrogen	5.3
Nitrogen	0.7
Sulfur	< 0.02
Oxygen	52.6
<i>Heating value (MJ/kg)</i>	
Low	13.0
High	14.1
<i>Ash analysis (wt%, dry basis)</i>	
SiO ₂	42.0
Al ₂ O ₃	8.7
Fe ₂ O ₃	5.0
CaO	28.0
SO ₃	1.0
MgO	3.7
P ₂ O ₅	2.6
K ₂ O	6.9
Na ₂ O	0.6
Cl	0.6
Other oxides	0.9

is dominated by the thermal radiation from the char oxidation since there is no volatiles flame any longer to originate CH radicals. The thermal radiation signal is, however, negligible compared with the CH emission signal, which makes the BF430 filter suitable to examine the volatiles combustion process.

Similar to the CH radicals, the C₂ radicals are also an intermediate product that may be present in the reaction zone. The excited C₂ radicals can originate emission at around 515 nm. As can be seen in Fig. 2a, emission at 515 nm is also identified in the measured spectrum, but the signal is rather weak and has a low signal/noise ratio due to the strong background from the thermal radiation of the burning soot

particles. In this case, images were captured with the ICCD camera equipped with a band-pass filter with a central wavelength of 515 nm (BF515). Again, a doughnut shape flame front similar to that provided by the CH emission image can be identified in Fig. 2b for a residence time of 70 ms, despite the presence of a strong signal in the image presumably originated from the soot particles. For a particle residence time of 120 ms, it is noticeable the thermal radiation originated from the burning of the char particles.

Fig. 2a reveals that the strongest measured emission lines are located at 589 nm, 766 nm and 769 nm, originated from the excited atomic sodium (589 nm) and potassium (766 nm and 769 nm). Biomass fuels usually contain high amounts of alkali metals, especially potassium compounds (cf. Table 1). In the volatiles combustion stage of the burning pulverized wheat straw particles at a residence time of 70 ms (Fig. 2b), large amounts of excited atomic sodium and potassium are present around the particles. Moreover, Fig. 2a reveals that the strength of the atomic sodium and potassium emission is overwhelming as compared with the other ones. Fig. 2b shows the signal distribution obtained with the 589 nm band-pass filter (BF589) and the 766 nm band-pass filter (BF766) and reveals that, for a particle at a residence time of 70 ms, the regions with the highest intensities coincide with the flame front identified through the CH emission signal. Note that, in contrast with the CH and C₂ radicals, both the atomic sodium and potassium are not consumed in the flame front, which leads to its presence above the flame that surrounds the burning particle due to buoyancy effects. In the char oxidation stage of the burning pulverized wheat straw particles at a residence time of 120 ms (Fig. 2b), the images captured with the ICCD camera equipped with the filters BF589 and BF766 are significantly different from those captured with the other filters, with the strongest excited atomic sodium and potassium signal intensities surrounding the burning particles. Unlike the images captured during the volatiles combustion stage, during the char oxidation stage the signal is symmetrically distributed, which indicates that the buoyancy effects in this stage are insignificant and that the released atomic sodium and potassium are rapidly oxidized by the ambient oxygen.

The 652 nm band-pass filter (BF652) was used to obtain information on the distribution of the soot particles. Based on the image captured with the ICCD camera equipped with the filter BF515 for a residence

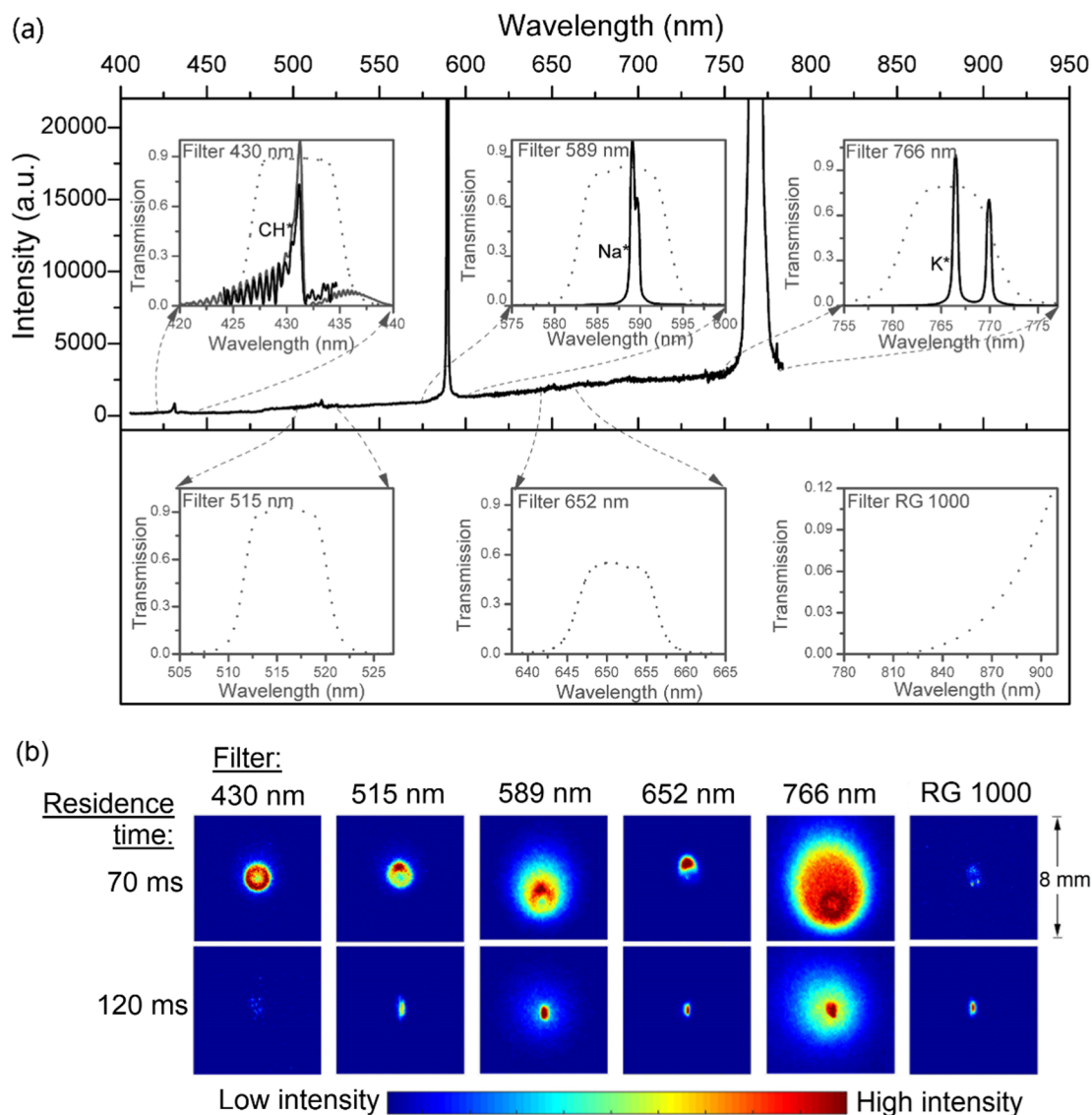


Fig. 2. (a) Emission spectrum of burning pulverized wheat straw particles obtained with the spectrometer, with detailed spectral structure of selected portions (black solid lines in the insets) and transmission curves of the corresponding filters (grey dot lines in the insets). The grey solid line in the inset for filter 430 nm is a simulated emission spectrum of CH^* using LIFBASE [13]. (b) Typical images of burning pulverized wheat straw particles obtained with the ICCD camera equipped with different filters for particle residence times in the hot combustion products region of 70 and 120 ms.

time of 70 ms, it can be concluded that the strongest signal intensity in the image obtained with the ICCD camera equipped with filter BF652, located above the burning particle, originated from the accumulation of incomplete oxidized hydrocarbons due to buoyancy effects. In addition, a long-pass filter (RG 1000) was used to obtain the broad-band emission in the infra-red wavelength region. The corresponding images shown in Fig. 2b reveal that the thermal radiation intensity from the burning of the soot particles in the infra-red wavelength region is weaker than that from the burning of the char particles, which makes the RG 1000 filter suitable to investigate the char oxidation process.

3.2. Particle burning process

Fig. 3 shows sequences of instantaneous images of burning pulverized wheat straw particles obtained with the ICCD camera equipped with five pairs of filters. In order to gather information on the combustion process of each biomass particle from ignition to the early stages of the char oxidation, the imaging region of the ICCD camera was set to 60 mm \times 60 mm with a spatial resolution of $\sim 58 \mu\text{m}$ per pixel. The location of the imaging region above the burner was set in two

ways: (i) from 0 (burner surface) to 60 mm above the burner surface, or from 30 mm to 90 mm above the burner surface, as shown in Fig. 3. When a particle was injected upward into the confined hot combustion products region, the ICCD camera was triggered and generated a burst of 14 pulses. The time gap between each pulse was 10 ms and the camera exposure time for each pulse was 500 μs . As mentioned earlier, a stereoscope lens was placed in front of the camera to allow for the simultaneous capture of images of each particle with two filters. The filter BF430 was chosen to pair with the other five filters (BF515, BF589, BF652, BF766 and RG 1000). The residence time of each particle was calculated based on its mean velocity and position above the burner. The mean velocity of the burning biomass particles during the volatiles combustion stage was around 0.6 m/s, as shown in the dashed marked region of Fig. 4. It is interesting to observe that the velocity of the particles is always higher than that of the flue gas (~ 0.42 m/s). The velocity of the nitrogen flow that transports the particles through the burner central hole is ~ 0.8 m/s. After injection into the hot combustion products, the velocity of the particles decreases slightly from ~ 0.7 m/s down to ~ 0.55 m/s, beyond which it increases up to ~ 0.95 m/s. While the initial small decrease in the velocity of the particles is expected, the

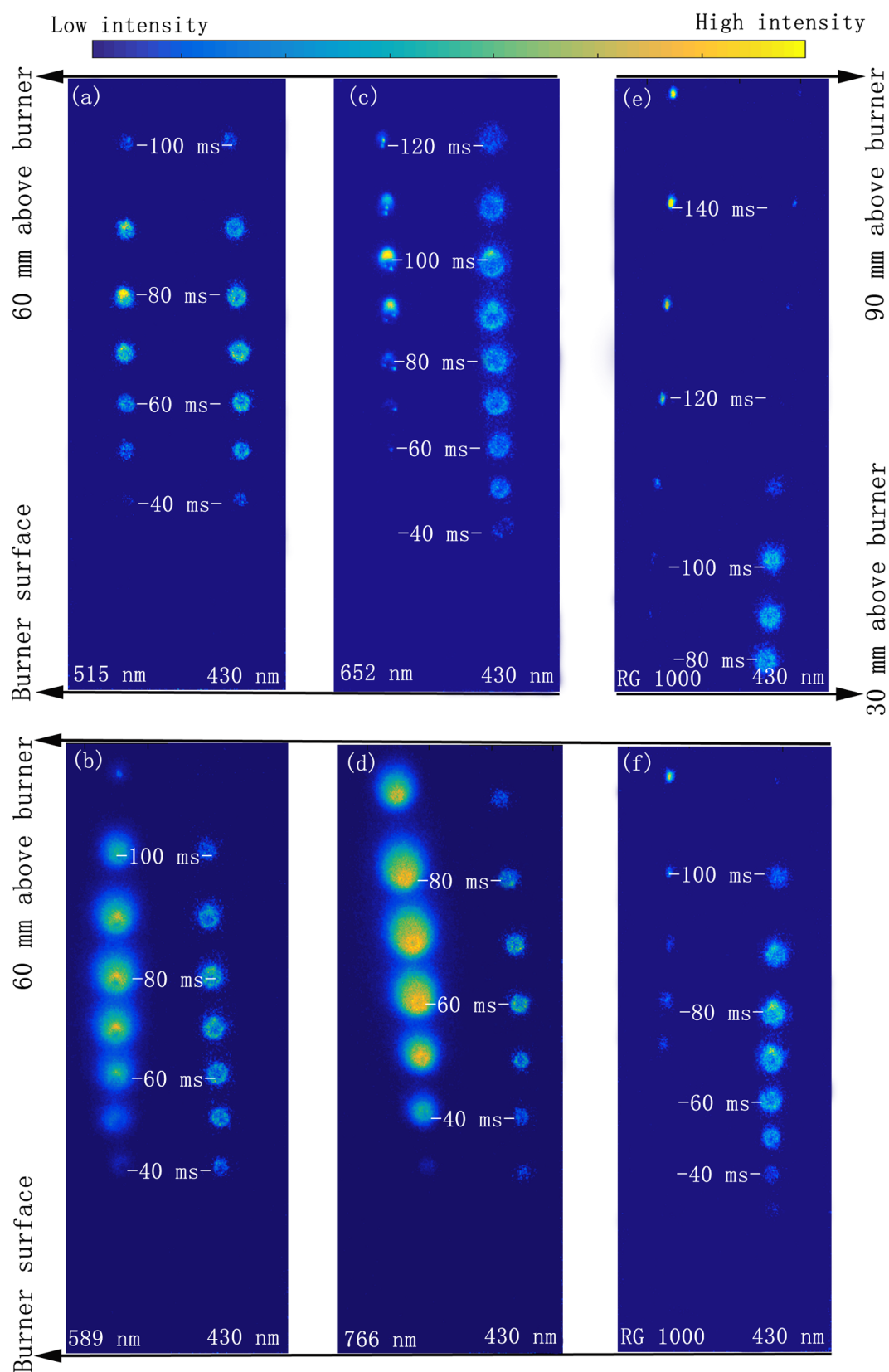


Fig. 3. Sequences of instantaneous images of burning pulverized wheat straw particles obtained with the ICCD camera equipped with five pairs of filters. (a) 515 nm and 430 nm; (b) 589 nm and 430 nm; (c) 652 nm and 430 nm; (d) 766 nm and 430 nm; (e and f) RG 1000 and 430 nm. Information on the particle residence time in the hot combustion products region is included in the panels of the figure.

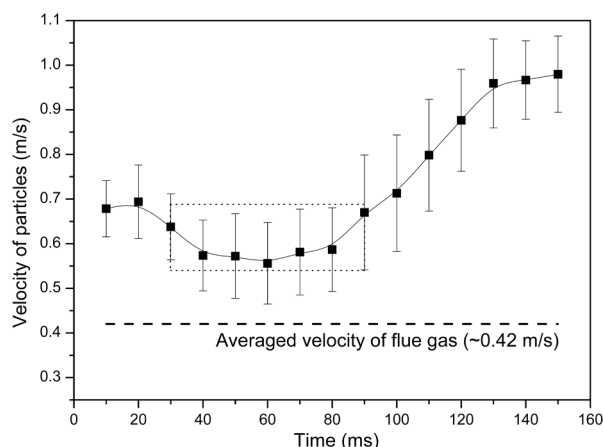


Fig. 4. Particle velocity as a function of the residence time. Error bars derived from 600 particles.

subsequent increase can be attributed to the combustion of the volatiles and associated heat release, which increases the gas temperature around the particle and thereby the particle velocity.

It should be mentioned that detailed axial temperature profiles are reported elsewhere [12]. For the condition used in this study the on-axis gas temperature rapidly reached ~ 1550 K, which remained approximately constant up to residence times of ~ 100 ms.

The images in Fig. 3 reveal that the emission from excited CH, C_2 , Na and K start to be detected almost at the same time (between 30 and 40 ms), which might be used as a criterion for the volatiles ignition (see below). Subsequently, the flame expands to a maximum, and then burns out. The burning of the soot particles initiates between 20 and 30 ms after the volatiles ignition (cf. Fig. 3c).

Fig. 3f indicates that soot burning extends up a particle residence time of 100 ms. Beyond this residence time (100 ms), Fig. 3e and f show that the thermal radiation signal intensity increases again, no doubt due to the onset of the char oxidation process, which reveals that the char particles experience ignition after the extinction of the homogeneous combustion. This is clearly seen in Fig. 5, which shows three single measurements of the emission signal intensity of burning pulverized wheat straw particles obtained with the ICCD camera equipped with 430 nm and RG 1000 filters as a function of the particle residence time in the hot combustion products region. The significant increase in the thermal radiation emission around a residence time of 100 ms confirms the observations above in regard to the beginning of the char oxidation

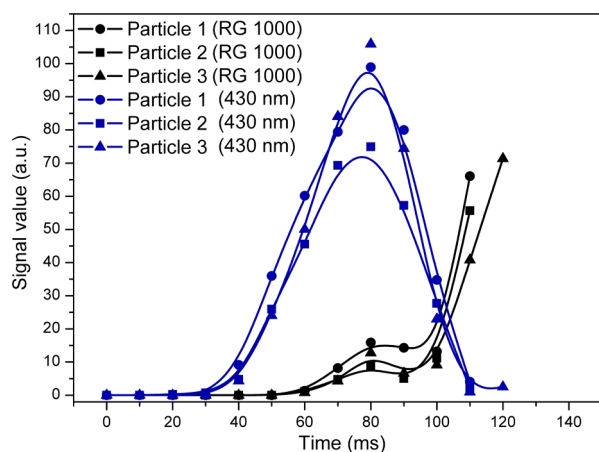


Fig. 5. Three single measurements of the emission signal intensity of burning pulverized wheat straw particles obtained with the ICCD camera equipped with 430 nm and RG 1000 filters as a function of the particle residence time in the hot combustion products region.

process.

Fig. 6 shows the normalized emission signal intensity of burning pulverized wheat straw particles obtained with the ICCD camera equipped with five pairs of filters as a function of the particle residence time in the confined hot combustion products region. The data is based on measurements for 100 particles for each pair of filters. Note that the emission intensity is expressed as both the total signal value (SV) and as the image signal area (SA).

Fig. 6a shows the data obtained with the ICCD camera equipped with the pair of filters BF515 and BF430, which indicate predominantly the emission of excited C_2 and CH, respectively. The evolution of the normalized emission signal intensity with the residence time for both filters is quite similar. In both cases, emission starts to be detected for a particle residence time in the hot combustion products region of ~ 20 ms (ignition point); subsequently, emission intensity increases up to a maximum located at ~ 70 ms, due to the intense combustion of the volatiles, beyond which it diminishes down to values close to zero for a particle residence time of ~ 130 ms. The small differences observed between the BF515 and BF430 curves are mainly caused by the interference of the thermal radiation from the burning of the particles of soot and char. In the period of time between 20 and 70 ms, where only volatiles combustion occurs, the influence of the broad-band emission originates mostly from the thermal radiation of the soot oxidation. Despite the higher signal intensity measured with the filter BF515 than with the filter BF430 (cf. Fig. 2b), the influence on the signal area is quite small, as seen in Fig. 6a. Beyond a residence time of around 100 ms, where char oxidation starts, as discussed above, Fig. 2b reveals the strong radiation generated, especially in the long wavelength region, which again explains the higher signal intensity measured with filter BF515 than with filter BF430 (cf. Fig. 6a).

Fig. 6b and d show the data obtained with the ICCD camera equipped with the pair of filters BF589 and BF430, and pair of filters BF766 and BF430, which allow to observe the temporal evolution of the emission intensity of the excited atomic sodium and potassium, respectively. During the volatiles combustion stage, the emission intensity of the excited atomic sodium and potassium increase in a way similar to that of the CH emission intensity; during the char oxidation stage, however, the decrease of the emission intensity of the excited atomic sodium and potassium, especially the signal area, presents a different behavior. In these cases, the decrease of the emission intensity of the excited atomic sodium and potassium is delayed in relation to the decrease in the emission intensity of CH because of the continuous release of atomic sodium and potassium from the burning char particles.

Fig. 6c shows the data obtained with the ICCD camera equipped with the pair of filters BF652 and BF430, with the former providing information on the distribution of the soot particles. It is seen that soot oxidation initiates ~ 20 ms later than ignition of the volatiles, as typified by the CH emission intensity curve, reaching a maximum also ~ 20 ms later than the maximum of the CH emission intensity. Beyond a residence time of ~ 100 ms, the thermal radiation signal originated from the burning char particles augments due to the enhanced char oxidation.

Fig. 6e shows the data obtained with the ICCD camera equipped with the pair of filters RG 1000 and BF430, with the former providing more information on thermal radiation, especially during the char oxidation stage since the signals from the char burning particles are much stronger than those from the oxidation of the soot particles. This means that the RG 1000 curves can be used as an indicator of the evolution of the char oxidation process.

Finally, Fig. 6f compares the temporal evolution of the emission intensity of the CH for cases (a) to (e). Using a criterion of 15% of the maximum CH emission intensity to define the ignition delay time for the present wheat straw particles under the studied conditions a value of 30 ms is obtained. This value is in line with the value reported by Simões et al. [12] for the same biomass residue in the same experimental setup but using an ignition criterion based on the visible light

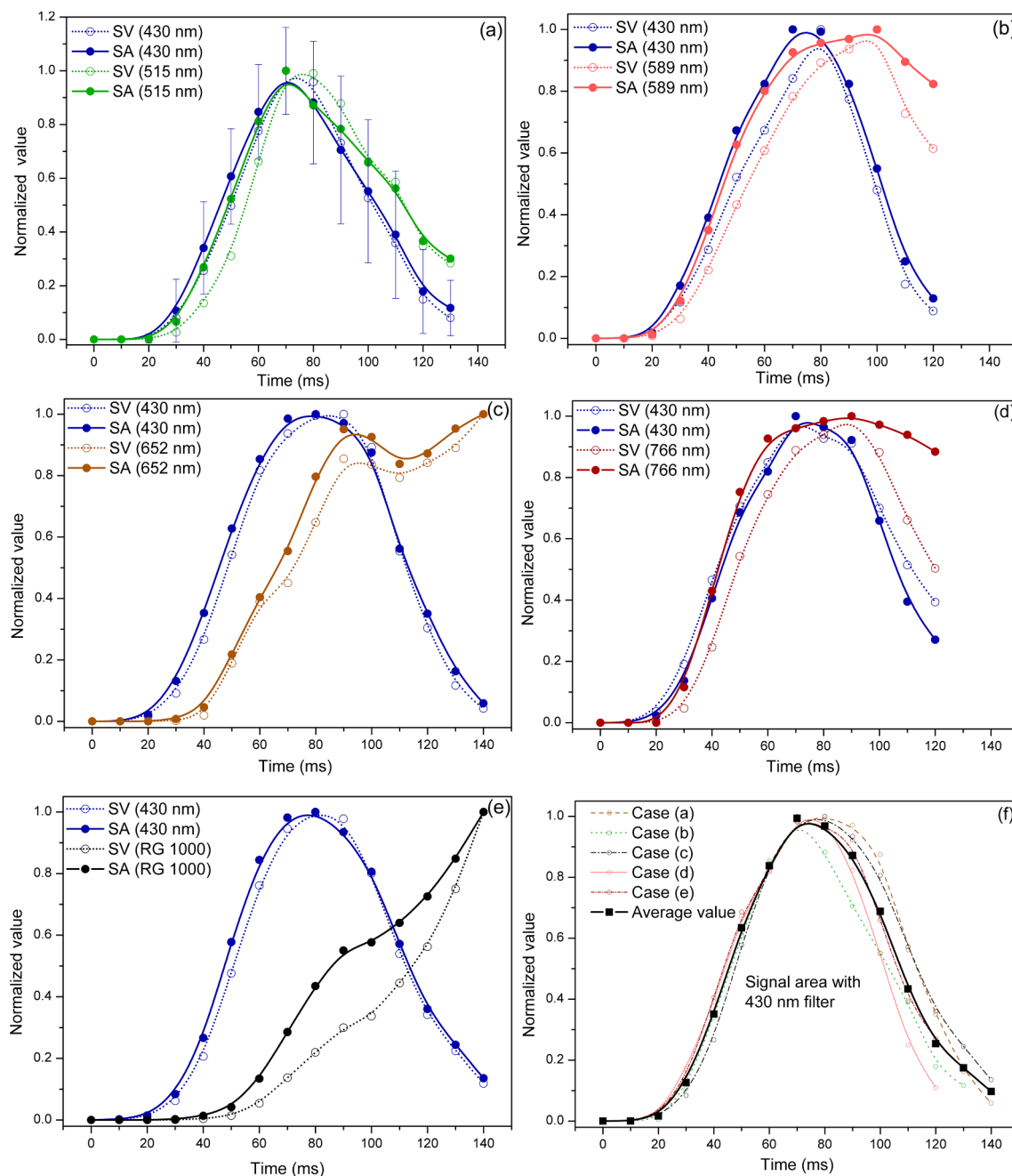


Fig. 6. Normalized emission signal intensity of burning pulverized wheat straw particles obtained with the ICCD camera equipped with five pairs of filters as a function of the particle residence time in the hot combustion products region. (a) 430 nm and 515 nm; (b) 430 nm and 589 nm; (c) 430 nm and 652 nm; (d) 430 nm and 766 nm; (e) 430 nm and RG 1000. The emission intensity is expressed as both the total signal value (SV) and as the image signal area (SA). (f) Emission intensity of the signal area taken with the 430 nm filter for cases (a) to (e). Error bars derived from 100 particles.

signal (15% of the maximum luminosity intensity).

4. Conclusions

Single particles of wheat straw in the size range 224–250 μm were injected upward into a confined region with hot combustion products, produced by a flat flame McKenna burner, with a mean temperature of 1550 K and a mean dry O_2 concentration of 6.5 vol% in order to evaluate their combustion behavior from ignition to the char oxidation early stages. Spectral emission data and temporally resolved images of the single burning particles were obtained with a spectrometer and an ICCD camera, respectively. Overall, the results demonstrate the ability of the present experimental setup and the associated optical diagnostics

to gather quantitative information of the combustion process of single pulverized solid fuel particles. The emission spectrum from the burning particles showed that the emission was mainly due to the chemiluminescence from excited CH , C_2 , Na and K , and the grey/black body emission from soot particles and burning char particles. The ICCD images show that the emission from excited CH , C_2 , Na and K is initially detected almost at the same time (between 30 and 40 ms), the burning of the soot particles initiates between 20 and 30 ms after ignition, and the char particles experience ignition after the extinction of the homogeneous combustion, as clearly indicated by the thermal radiation emission, which is a good indicator of the char oxidation process. During the volatiles combustion stage, the temporal evolution of the normalized emission intensity of the excited CH , C_2 , atomic sodium and

atomic potassium is similar; during the char oxidation stage, however, the decrease of the emission intensity of the excited atomic sodium and potassium is delayed in relation to the decrease in the emission intensity of CH and C₂ because of the continuous release of atomic sodium and potassium from the burning char particles.

Acknowledgements

This work was supported by the Swedish Energy Agency through CECOST, the Knut and Alice Wallenberg foundation through grant KAW 2015.0294 and the European Research Council through Advanced Grant TUCLA, and by the Portuguese Fundação para a Ciência e a Tecnologia through IDMEC, under LAETA, project UID/EMS/50022/2013 and project PTDC/EMS-ENE/5710/2014. M. Costa also acknowledges FCT for the sabbatical leave grant SFRH/BSAB/128236/2016.

References

- [1] Shaddix CR, Molina A. Particle imaging of ignition and devolatilization of pulverized coal during oxy-fuel combustion. *Proc Combust Inst* 2009;32:2091–8.
- [2] Khatami R, Stivers C, Levendis YA. Ignition characteristics of single coal particles from three different ranks in O₂/N₂ and O₂/CO₂ atmospheres. *Combust Flame* 2012;159:3554–68.
- [3] Maffei T, Khatami R, Pierucci S, Faravelli T, Ranzi E, Yiannis A, Levendis YA. Experimental and modeling study of single coal particle combustion in O₂/N₂ and oxy-fuel (O₂/CO₂) atmospheres. *Combust Flame* 2013;160:2559–72.
- [4] Riaza J, Khatami R, Levendis YA, Álvarez L, Gil MV, Pevida C, et al. Single particle ignition and combustion of anthracite, semi-anthracite and bituminous coals in air and simulated oxy-fuel conditions. *Combust Flame* 2014;161:1096–108.
- [5] Khatami R, Levendis YA, Delichatsios MA. Soot loading, temperature and size of single coal particle envelope flames in conventional- and oxy-combustion conditions (O₂/N₂ and O₂/CO₂). *Combust Flame* 2015;162:2508–17.
- [6] Khatami R, Levendis YA. An overview of coal rank influence on ignition and combustion phenomena at the particle level. *Combust Flame* 2016;164:22–34.
- [7] Köser J, Becker JG, Goßmann AK, Böhm B, Dreizler A. Investigation of ignition and volatile combustion of single coal particles within oxygen-enriched atmospheres using high-speed OH-PLIF. *Proc Combust Inst* 2017;36:2103–11.
- [8] Bai X, Lu G, Bennet T, Sarroza A, Eastwick C, Liu H, et al. Combustion behavior profiling of single pulverized coal particles in a drop tube furnace through high-speed imaging and image analysis. *Exp Therm Fluid Sci* 2017;85:322–30.
- [9] Riaza J, Khatami R, Levendis YA, Álvarez L, Gil MV, Pevida C, et al. Combustion of single biomass particles in air and in oxy-fuel conditions. *Biomass Bioenergy* 2014;64:162–74.
- [10] Mock C, Lee H, Choi S, Manovic V. Combustion behavior of relatively large pulverized biomass particles at rapid heating rates. *Energy Fuels* 2016;30:10809–22.
- [11] Mock C, Lee H, Choi S, Manovic V. Flame structures and ignition characteristics of torrefied and raw sewage sludge particles at rapid heating rates. *Fuel* 2017;200:467–80.
- [12] Simões G, Magalhães D, Rabaçal M, Costa M. Effect of gas temperature and oxygen concentration on single particle ignition behavior of biomass fuels. *Proc Combust Inst* 2017;36:2235–42.
- [13] LIFBASE (version 2.1), <https://www.sri.com/contact/form/lifbase>.